Disruption of Capn15 in mice leads to brain and eye deficits

Congyao Zha[1]#, Carole A Farah[1]#, Vladimir Fonov[1], Richard Holt[2], Fabiola Ceroni[2], Nicola Ragge[2, 3], David Rudko[1], and Wayne S Sossin[1]*

[1]*Department of Neurology and Neurosurgery, Montreal Neurological Institute, McGill University, Montreal, Quebec, Canada, H3A 2B4*

[2] *Faculty of Health and Life Sciences, Oxford Brookes University, Oxford, OX3 0BP, UK*

[3] *West Midlands Regional Clinical Genetics Service and Birmingham Health Partners, Birmingham Women's and Children's NHS Foundation Trust, Birmingham, B15 2TG, UK*

#Equally contributed

*Corresponding author: Wayne S Sossin; Email: wayne.sossin@mcgill.ca

Abstract

The murine Calpain 15 (Capn15) is an intracellular cysteine protease that belongs to the non-classical Small Optic Lobe (SOL) family of calpains. SOL calpains lack the penta-EF-hand structure found in classical calpains, but have N-terminal Zinc Fingers that bind polyubiquitin and a C-terminal SOL domain with poorly characterized function. In this study, we have generated *Capn15* transgenic mice and taking advantage of the lacZ reporter under the control of the *Capn15* promoter, show that *Capn15* is highly expressed in the developing brain and is enriched in the eyes, the superficial cortical layers, the hippocampus, and the Purkinje cells in the cerebellum in the adult. The homozygous loss of Capn15 decreases embryonic survival and weaned mice have smaller brains and weigh less than their WT littermates. MRI studies revealed specific volume losses in the superior parietal cortex and thalamus and in the CA1, CA2, dentate gyrus and stratum granulosum in the hippocampus. Most importantly, *Capn15* KO mice had mild to severe eye deficits that ranged from cataracts to microphthalmia (small eye) and anophthalmia (no eye). We further identify a missense homozygous variant of *CAPN15* in one patient from a UK cohort with ocular anomalies indicating a potential link between *CAPN15* and microphthalmia in humans. Surprisingly, knocking-out the atypical PKC/PKMζ in *Capn15* KO mice rescues the severe eye deficits in these mice suggesting that cleavage of PKCζ by Capn15 may play an important role in eye development.

Introduction

Calpains are intracellular cysteine proteases that were first discovered in rat brain (1). There are four conserved families of calpains: Classical, PalB (phosphatase mutants: loss in activity at alkaline pH, but normal or increased activity at acidic pH), Transformer (Tra), and Small Optic Lobe (SOL) with the classical being the best characterized calpains. All calpain isoforms have a conserved catalytic domain and each calpain family has unique domains: a C-terminal penta-EF hand domain in classical calpains; a C-terminal C2 domain in Tra calpains; an N-terminal MIT domain and an additional C-terminal C2 like domain in PalB calpains, and an N-terminal zinc finger domain that binds polyubiquitin (2) and a C-terminal SOL homology domain in SOL calpains (3, 4).

Calpains play diverse roles in cellular physiology. For instance, degradation of repressors of plasticity by calpain in the hippocampus is important for induction of synaptic plasticity associated with memory (5-7). Calpains play roles in apoptosis (8), cytoskeletal remodelling (9, 10), transcriptional activation (11) and many other physiological and pathological processes (12-16). Calpains were also shown to play important roles in development. As such, homozygous disruption of the murine classical calpain small subunit gene *Capn4* led to disruption of the activities of classical calpains Capn1 and Capn2 and mutant embryos died at midgestation and displayed defects in the cardiovascular system, hemorrhaging, and accumulation of erythroid progenitors (17). Furthermore, homozygous *Capn2* deletion resulted in pre-implantation embryonic lethality between the morula and blastocyst stage (18). Tra-3 (Transformer 3) calpain was first discovered in the nematode *C. elegans*, as a sex determination gene (19). Later, studies suggested that Tra-3 cleaves Tra-2, which then interacts with transcription factor

Tra-1 both directly and indirectly to promote female development (20, 21). In addition, a single nucleotide polymorphism in *Tra-3* resulted in smaller body size in *C. elegans* grown at low temperature (22). In humans, mutations in the orthologue of the Tra calpain (*CAPN5*) that hyperactivate its protease activity lead to inflammatory vitreoretinopathy, hearing loss and developmental delay (23). PalB was identified in the fungus *Aspergillus nidulans*, as a protease involved in the alkaline ambient pH signal transduction pathway (24). In an alkaline ambient environment, PalB is required for cleavage and activation of transcription factor PacC (25) that in turn activate genes adaptive to alkaline environment.

SOL calpain was first characterized in the fruit fly *Drosophila* (26, 27). Loss of SOL calpain leads to a 50% reduction in the volume of *Drosophila* optic lobes due to degeneration and absence of certain classes of columnar neurons (27). In humans, *SOLH* was mapped to chromosome position 16p13.3 (28) which is a region potentially carrying genes involved in CATM (hereditary cataracts with microphthalmia) (29). However, how SOL calpain is activated and the identity of its substrates remains unknown. While calcium can activate classical calpains by binding to their unique classical penta-EF hand domain and their catalytic domain (30) and can also activate atypical calpains such as Tra by binding to the catalytic domain (20), it was shown to have no detectable effect on SOL calpain activity (2). This is most probably due to the lack of conservation of calcium binding residues in the catalytic domain of SOL calpain (2). In addition, while the SOL calpain zinc finger domain binds to polyubiquitin, polyubiquitin alone or together with calcium did not activate SOL calpain (2).

Protein kinase Ms (PKMs) are truncated version of protein kinase Cs (PKCs) that only contain the catalytic domain. Various studies using different model organisms have

proven that PKMs are vital to memory maintenance (31-38). While the vertebrate PKMζ can be generated by an alternative transcript that encodes the catalytic domain of PKCζ (39), this transcript is chordate specific and PKMs are produced by calpain-dependent cleavage of PKCs in invertebrates (40-42). Furthermore, experiments in sensorimotor co-cultures of the marine mollusk *Aplysia californica* have shown that inhibiting different forms of calpains using dominant negative constructs can block different forms of plasticity (43). Indeed, inhibiting classical calpain blocked the induction of associative long term facilitation while inhibiting SOL calpain blocked the induction of non-associative long term facilitation (43); long term facilitation being the cellular analog of long term sensitization behaviour in the animal.

The role of SOL calpain (Capn15) has not been characterized in vertebrates. In this study, we have generated *Capn15* knockout mice. By taking advantage of a lacZ reporter gene under the control of the *Capn15* promoter, we show that Capn15 is enriched in the eyes, the superficial cortical layers, the hippocampus, and the Purkinje cells in the cerebellum. We also find that *Capn15* expression levels are higher during early development and loss of *Capn15* results in a lower Mendelian ratio and lower weight in mice. Furthermore, *Capn15* KOs have overall smaller brains, with particular increased losses in thalamus and sub-regions of the hippocampus. Most importantly, *Capn15* KO mice have cataracts, microphthalmia and anophthalmia consistent with *CAPN15* being a locus of CATM for humans. We also present a human patient with unilateral microphthalmia, bilateral colobomas and mild lens opacity carrying a homozygous missense variant in *CAPN15* that is absent from public databases. Together,

these findings support a role for *CAPN15* in neurodevelopment and congenital eye anomalies.

Material and methods

Capn15 antibody Polyclonal antibodies were raised in rabbits against the carboxy terminal of Capn15 using the following epitope: CDVAGLHGPRPL. A cysteine residue was added to the N-terminal of the peptide to enhance coupling. Peptides were coupled to KLH-maleimide and SulfoLink coupling resin (Thermo scientific) according to manufacturer's instruction. After conjugation to KLH-maleimide, rabbits were injected and after four boosts the final serum was affinity purified on SulfoLink columns as previously described (44).

Dissections Adult mice were transcardially perfused with ice-cold phosphate-buffered saline (PBS) followed by 4% (wt/vol) ice-cold paraformaldehyde (PFA) in phosphate-buffered saline (PBS). Brains were post-fixed in 4%PFA for 45min at 4℃, rinsed in PBS, and cryoprotected in 30% sucrose/PBS overnight at 4℃. On the next day, brains were embedded in OCT (Fisher Healthcare) and flash frozen in 2-methylbutane chilled in dry ice. The brains were kept at −80°C until further use. For amygdala dissection, mouse brains were removed and frozen on dry ice. The brains were kept at −80°C until further use. The amygdala was dissected from each frozen brain in the cryostat using a neuro punch (0.5 mm; Fine Science Tools). For MRI analysis, adult mice were transcardially perfused with ice-cold PBS followed by 4% (wt/vol) ice-cold PFA in

PBS. Brains were then post-fixed in 4% PFA overnight at 4℃, rinsed in 1XPBS, and stored in 1XPBS + 0.05% sodium azide.

X-gal staining Sections were incubated overnight at 37°C in solution containing 80 mM Na_2HPO_4, 20 mM NaH_2PO_4, 2 mM $MgSO_4$, 5 mM potassium ferricyanide, 5 mM potassium ferrocyanide, 0.2% NP-40, 0.1% sodium deoxycholate, and 1.5 mg/ml X-gal. Sections were rinsed in PBS, washed in ethanol, cleared in xylene, and mounted with Permount (Fisher Scientific).

Western blotting Embryonic brains were homogenized manually in lysis buffer containing 25mM Tris-HCl (pH 7.4), 150mM NaCl, 6mM MgCl2, 2mM EDTA, 1.25% NP-40, 0.125% SDS, 25mM sodium fluoride, 2mM sodium pyrophosphate, 1mM dithiothreitol (DTT), 1mM phenylmethylsulfonyl fluoride, 20 mg/ml leupeptin, and 4 mg/ml aprotinin by pestles. Before loading, 5X sample buffer was added to the lysate and samples were boiled at 95°C for 5 min. Proteins were resolved by SDS-PAGE on Bis-Tris gel and transferred to nitrocellulose membrane (Bio-Rad). The blots were blocked in TBST (TBS + 0.1% Tween) containing 4% skim milk for 30 min at room temperature and then incubated with primary antibodies overnight at 4°C. After washing 3 times with TBST, the blots were incubated with HRP-conjugated secondary antibodies for 1 hour at RT, washed again for 3 times in TBST. Western Lightning Plus- ECL kit (NEL103001EA; PerkinElmer LLC Waltham, MA USA) was used as per manufacturer's instructions to detect protein bands. The primary antibody used was homemade rabbit anti-Capn15 antibody (1:1000) that we raised against the C-terminus of Capn15. The

secondary antibody used was horseradish peroxidase-conjugated goat anti-rabbit secondary antibody (1:5000). Antibodies were diluted in Tris buffered saline with Tween containing 4% skim milk powder.

Quantification of immunoblotting Immunoblots were scanned and imaged using the public domain Image J program (developed at the U.S. National Institute of Health and available on the Internet at https://imagej.nih.gov/ij/). We calibrated our data with the uncalibrated optical density feature of NIH image, which transforms the data using the formula $\log_{10}[\frac{225}{225-x}]$, where x is the pixel value (0–254). We find that with this correction and including the entire band (which expands near saturation), that values are linear with respect to amount of protein over a wide range of values (45). We first normalized the amount of SOL calpain using the Ponceau image. To be able to use different blots, we always normalized the amount of SOL calpain in brains at different ages to the amount of SOL calpain in E12-E14 brains run on the same gel.

Image Acquisition Magnetic resonance imaging was performed using the 7 T Bruker Pharmascan (Bruker Biosciences, Billerica, MA) ultra-high field MRI system of the McConnell Brain Imaging Centre. For imaging, brains were housed in a cylindrical container and immersed in an MR-invisible fluorinated solution, FC-40 (Sigma Aldrich, St. Louis, Missouri), to remove the background MRI signal. For MRI radiofrequency excitation and reception, a 2.3 cm inner diameter volume resonator was utilized. The imaging protocol included a sagittal orientation, 3D steady-state free precession MRI sequence with an echo time (TE) of 5 milliseconds, repetition time (TR) of 10

milliseconds, receiver bandwidth of 50 kHz and excitation pulse flip angle of 30 degrees. The image acquisition matrix was selected to achieve an isotropic voxel resolution of 100 μm^3. The specific sagittal orientation imaging field of view was $2.3 \times 1.7 \times 1.7$ cm^3. 31 signal averages were collected to improve image signal-to-noise ratio, leading to a total scan time of approximately six hours and 60 seconds for the full MRI histology scan. For image reconstruction, a trapezoidal filter was applied to the complex image data along the first phase encode direction to reduce subtle effects of Gibbs ringing.

Image Processing and Statistical Analysis We employed an image registration-based method to investigate anatomical brain volume differences between wild type (WT), conditional knockout (cKO) and full knockout (KO) mice. Specifically, an automated, image intensity-based, affine registration (46) was used to align all mouse brains to a common coordinate system. During this registration step, it was determined that the KO mouse brains were, on average, 14% smaller than the WT mouse brains. For this reason, as part of the affine registration, a volumetric pre-scaling was applied to globally scale the KO brain images by a factor of 1.14. The pre-scaling used a nearest neighbour approach. To avoid registration bias caused by differences between our studied population and the mouse template (47), a population-specific average was constructed using an algorithm described in Fonov et al (48). This step yielded an average image of all the samples included in our cohort. A mouse brain atlas (47) containing reference regions of interest (ROIs) for the thalamus, amygdala, parieto-temporal cortex and whole hippocampus was next used to provide suitable ROIs for volumetric measurement. More specifically, a non-linear registration (ANTs (49)) between the atlas space (47) and our

population average was conducted to create an anatomical atlas specific to our mouse population. The deformation fields from the non-linear registration were inverted and blurred with a Gaussian smoothing kernel. The Jacobian determinants of the deformation fields were then extracted to yield estimates of local expansion or contraction at both the ROI and voxel level relative to the population average. Since we also had a specific interest in volumetric changes in KO mice in the hippocampal sub-fields, a mouse hippocampal sub-field atlas (50) was non-linearly registered (49) and warped to the population average to measure volumes of the cornu ammonis 1 (CA1), CA2, CA3, stratum granulosum and dentate gyrus in the mouse brain images.

We next used a linear model in the R software package (51) to measure the main effect of volume differences (i) in individual ROIs in KO and cKO mice compared to WT mice and (ii) at the voxel-level in KO and cKO mice compared to WT mice. All statistical analyses were corrected for multiple comparisons, utilizing the false discovery rate technique (52) with a 5% threshold.

Patient Cohort Description A UK cohort of 316 individuals with ocular anomalies, principally AMC, was recruited as part of a national 'Genetics of Eye and Brain anomalies' study (REC 04/Q0104/129). Informed consent was obtained according to the tenets of the Declaration of Helsinki. Patients were screened by indication in known AMC genes.

Whole Exome Sequencing Fifty-six individuals from 55 families within the cohort were screened by whole exome sequencing (WES) as described previously (53, 54)

Results

Generation of Capn15 KO mice

Embryonic stem cells with a cassette inserted into the mouse *Capn15* locus (intron 2) were obtained from the International Mouse Phenotyping Consortium (IMPC). The strategy used by the consortium was to insert a cassette that provides a strong exon entry site coupled with a stop codon with lacZ produced from internal ribosome entry site translation (55, 56). To remove the lacZ-Neo cassette, these mice were bred with mice that contain flippase (FLP) recombinase that recognizes a pair of Flp recombinase target (FRT) sequences that flank the genomic region containing this cassette (Fig.1A) leaving lox sites surrounding the catalytic exons 3-5. These mice were then either bred against mice expressing germline Cre recombinase to remove the floxed exons and generate a KO line or bred with the CaMKIIα-Cre-CRE T29-1 (57) to generate a conditional KO mouse that only knocks out *Capn15* after development in forebrain excitatory neurons (Fig.1A).

In order to validate Capn15 disruption, we raised an antibody against the C-terminal of Capn15. Embryonic brains were homogenized and run on SDS gels and western blotting was performed as described in Methods. A band of ~130kDa corresponding to the expected molecular weight of Capn15 was detected in brain homogenates from wild type mice (Fig.1B, *Capn15*$^{+/+}$). The levels of this band were reduced in *Capn15* heterozygous mice (*Capn15*$^{+/-}$) and the band was undetectable in *Capn15* KO mice (*Capn15*$^{-/-}$) demonstrating both the usefulness of the antibody and the complete KO of the protein. As the antibody is raised to the C-terminal, we cannot rule

out truncated products (consisting of the N-terminal zinc finger domain) remaining in the KO.

Capn15 developmental expression

Capn15 was first identified in *Drosophila* as its mutation led to small optic lobes (26). There is a single well -conserved member of this calpain family in all metazoans and the SOL calpains diverged from the other calpains near the time that fungi and metazoans diverged (4). To gain better insight into *Capn15* role in the mouse brain, we took advantage of the reporter gene lacZ which expression is controlled by the *Capn15* promoter to investigate whether Capn15 was enriched in different brain areas during development. X-gal staining of sagittal sections of E12 embryos showed that *Capn15* was mainly expressed in the outer layer of the central nervous system, also known as the mantle zone (Fig.2A). In E18 brains, *Capn15* is largely expressed in the subventricular zone, immediately next to the ventricular zone (Fig.2A). *Capn15* expression was also observed in the deep cortical layer and neuroepithelium layer in hippocampus, but not the pyramidal layer. In newly born mice (P3), *Capn15* is ubiquitously expressed in the brain, from the olfactory bulb to the cerebellum and staining of P3 mice eyes showed that *Capn15* was also enriched in the different layers of the retina (Fig.2A). However in adult mice, while *Capn15* expression is remarkably reduced, demonstrated by an overall weakening in X-gal staining, *Capn15* retains its expression in specific areas, such as layer II/III of the cortex, excitatory pyramidal neurons in CA1 and CA3 and some inhibitory neurons located in stratum radiatum (Fig.2A). In the dentate gyrus, *Capn15* is expressed in subgranular zone and it showed the strongest signal in the molecular layer of dentate

gyrus, mainly containing interneurons such as molecular layer perforant pathway cells (MOPP) (58) and neurogliaform cells (59)(Fig. 2A) . In the cerebellum, *Capn15* is most strongly expressed in Purkinje cells (Fig.2A).

Results from X-gal staining suggested stronger expression levels of *Capn15* in the developing brain. To confirm this, we examined *Capn15* expression in rat brain at different developmental time points as described in Methods. As shown in Figs.2B and 2C, Capn15 expression is strongest during embryonic development (E14-E18 brains) and its expression levels decrease significantly after birth (P0-adult) pointing to an important role for this calpain in brain development.

Capn15 KO mice have mild to severe eye deficits

To generate *Capn15* KO mice, we crossed *Capn15* heterozygous mice together with an expected Mendelian ratio of 25:50:25 in percentage (WT, het, KO). However, *Capn15* KO mice were not born at Mendelian ratio and only 12% of mice were KO from these crosses (p=1.28e-5, Chi Square test, strongly disagrees with Mendelian ratio; n=52 for the WT group, n=155 for the *Capn15*$^{+/-}$ group and n=29 for the *Capn15*$^{-/-}$ group; Fig.3A). Furthermore, *Capn15* KO mice that were successfully weaned weighed significantly less than their littermate WT or heterozygous mice (**p=0.003 and ***p=0.0006, Student's t-test; n=45 for the WT group, n=71 for the *Capn15*$^{+/-}$ group and n=18 for the *Capn15*$^{-/-}$ group; Fig.3B). Most importantly, as shown in Fig.3C, *Capn15* KO mice showed mild to severe deficits in eye development that ranged from cataract (31%) to microphthalmia (small or underdeveloped eye; ~26%) and the more severe anophthalmia (absent eye; ~18%). Both left and right eyes were assessed from adult

Capn15 KO mice and a Chi Square test revealed no significant difference between the 2 sides so both were combined for data analysis in Fig.3C (p=0.15). A Chi Square test revealed a significant difference in the distribution of the eye phenotype in *Capn15* KO mice compared to *Capn15* het or WT mice (***p<0.0001; n=30 for the WT group, n=160 for the *Capn15*$^{+/-}$ group and n=90 for the *Capn15*$^{-/-}$ group, this group also included offspring from parents who were both *Capn15*$^{-/-}$; Fig.3C). Moreover, a subset of mice was examined at earlier time points (6 and 12 weeks of age) with no difference in the eye phenotype detected indicating that these eye anomalies are also present in younger animals. To further test this, we generated *Capn15* conditional KOs (cKOs) as described above (Fig.1A) and a CaMKIIα-Cre line was used to this end. CaMKIIα-Cre transgenic mice have the mouse calcium/calmodulin-dependent protein kinase II alpha promoter driving Cre recombinase expression in a subset of excitatory neurons in the forebrain including the hippocampus and the amygdala and CRE is not expressed until after P14 (60). As shown in Figs.4A and 4B, Capn15 protein levels are significantly decreased in homogenates from *Capn15* cKO adult mice amygdala indicating successful disruption of the *Capn15* gene in cKO mice (**p=0.002, Student's t-test; n=4 cKO, 3 WT). Furthermore, a thorough assessment of these mice showed no weight difference compared to WT mice (p=0.16, Student's t-test; n=26 for the WT group composed of *Capn15* cKO Cre- littermates and n=15 for the cKO group; Fig.4C) and most importantly no eye deficits (Fig.4D, n=20 cKO, WT).

MRI analysis of Capn15 KO and Capn15 cKO adult brains

To determine whether removing Capn15 led to changes in brain volume, we performed whole brain MRI on 14 WT (9 M, 5F) and 8 *Capn15* KO (4M, 4F) animals. There was no difference in whole brain volume between male and female mice for either the WT (p=0.97) or the *Capn15* KO groups (p=0.83). Accordingly, males and females were grouped together for statistical analysis. All *Capn15* cKO mice (n=5) were males. There was a highly significant, 12% decrease in whole brain volume in the *Capn15* KO animals (p=7.32e-7) compared to the WT animals. We further noted a significant decrease in the hemisphere-averaged volume of the thalamus in *Capn15* KO animals compared to the corresponding WT animals (p=1.28e-5; Figs.5A and 5B) after compensating for the overall decrease in brain size (See Methods). There was no difference in thalamic volume between *Capn15* cKO and WT animals (p=0.35; Figs.5A and 5B). Atlas-based region of interest analysis revealed an increase in the amygdala volume of *Capn15* KO mice compared to WT mice (p=0.003, Figs.5A and 5B). However, there was no corresponding difference between *Capn15* cKO and WT mice (p=0.42). As well, there were no differences in volume of the parieto-temporal cortex between either *Capn15* KO or cKO mice and corresponding WT mice (Figs.5A and 5B). We also used voxel-based morphometry to measure local differences in volume between *Capn15* KO and WT mice. Twelve representative slices having locally decreased volume of *Capn15* KO brain compared to WT brain (blue colours) and the corresponding locally increased volume (yellow/orange colours) are presented in Fig.6. Volume decreases in *Capn15* KO mouse brain are notable (light blue colours) in the hippocampus, superior parietal cortex and thalamus.

Additional attention in our high resolution, MRI-based volume analysis was given to the hippocampus due to the possible role of Capn15 in synaptic plasticity (43, 61). An image of the hippocampal sub-field atlas we employed for sub-field volumetry is shown in Fig. 7A. We did not observe differences in overall hippocampal volume between either *Capn15* KO or *Capn15* cKO mice and the corresponding WT animals. However, voxel-level differences in hippocampal volume were observed between *Capn15* KO and WT mice when we restricted our linear model statistical analysis to regions inside the hippocampal sub-fields (Figs.7A and 7B). In particular, there were voxel decreases in hippocampal volume for mid-line slices of the *Capn15* KO mice brain compared to the WT mice. Examination of the hippocampal sub-fields using region of interest-based analysis identified decreases in the CA1 (p=0.001), the CA2 (p=0.002), the dentate gyrus (p=0.05) and the stratum granulosum (p=0.03) volume of *Capn15* KO mice when compared to WT mice (Figs.7A and 7B). Notably, such volumetric differences were not observed in CA3. As well, no differences in hippocampal sub-field volume were observed between *Capn15* cKO and WT mice.

A homozygous missense variant of Capn15 is found in one patient with microphthalmia

We next looked for a potential link between *CAPN15* and microphthalmia in humans. To this end, fifty-six cases (fifty-five independent families) from a UK cohort of individuals with ocular anomalies were screened by whole exome sequencing (WES), as described in Methods. One proband was found that carried a homozygous missense variant affecting the first nucleotide of exon 13 (NM_005632.2:c.2905G>A;

NP_005623.1:p.(Gly969Ser); chr16:602863 [hg19]). This variant is predicted damaging by SIFT and PolyPhen-2 and is absent from the gnomAD database (http://gnomad.broadinstitute.org/) (62-64). The variant was validated in the patient and confirmed to be present in the heterozygous state in both parents using Sanger sequencing.

The proband is a girl of Pakistani ethnicity with right iris and chorioretinal coloboma involving the disc and a mild lens opacity, and left mild microphthalmia with an iris and chorioretinal coloboma involving the disc. She is slightly hirsute with a low hairline at the front. At the time of the appointment she had a nasogastric tube due to gastrooesphageal reflux. She has a sacral dimple, had congenital pneumonia, monocytes anaemia, laryngeal cleft and dysphonia. She has poor weight gain since birth. Her parents are first cousins, both also born to consanguineous parents. She has two siblings, a brother with renal reflux and a congenital heart defect, and a sister with myopia and tachycardia. DNA was unavailable for both. The mother has bilateral cupped discs, calcium deficiency, iron deficiency, hyperthyroidism and lymphedema, and had multiple miscarriages and stillbirths. The maternal grandfather and aunt have glaucoma, but no other eye anomalies are present in the family. Other recurring problems in the family include thyroid problems, thalassemia traits and immune problems such as asthma and eczema. No other candidate variants to potentially explain the patient's phenotype were identified.

Knocking-out PKC/PKM Zeta in Capn15 KO mice rescues microphthalmia

We have previously shown that constitutive activation of PKCs through calpain mediated cleavage sustains long-term synaptic plasticity in *Aplysia* (40-43, 61). More specifically, in this system, non-associative long-term facilitation requires the SOL calpain (43). Due to the important role of PKM ζ in memory maintenance in vertebrates (65), we decided to explore a potential interaction between Capn15 and PKM ζ by knocking-out *PKC/PKMζ* in *Capn15* KO mice. First, we examined the eyes of *PKC/PKMζ*$^{(-/-)}$ mice and detected no obvious eye deficit (Fig.8A). However, while 15% of the *PKC/PKMζ*$^{(-/-)}$*Capn15*$^{(-/-)}$ mice had an obvious cataract, none of them had microphthalmia or anophthalmia (Fig.8A) and a Chi Square test revealed a significant difference in the distribution of the eye phenotype in the *PKC/PKMζ*$^{(-/-)}$*Capn15*$^{(-/-)}$ mice compared to *Capn15*$^{(-/-)}$ mice suggesting that knocking-out *PKC/PKMζ* suppresses the severe eye deficits observed in *Capn15*$^{(-/-)}$ mice (***p<0.0001, Chi Square test; n=38 for the *PKC/PKMζ*$^{(-/-)}$ group, n=90 for the *Capn15*$^{-/-}$ group and n=28 for the *PKC/PKMζ*$^{(-/-)}$*Capn15*$^{(-/-)}$ group, the *Capn15*$^{-/-}$ group is the same one used in Fig.3C). The *PKC/PKMζ*$^{(-/-)}$*Capn15*$^{(-/-)}$ mice examined in Fig.8A were generated from parents who were both *PKC/PKMζ*$^{(-/-)}$*Capn15*$^{(-/-)}$. To confirm these findings, we have crossed together *PKC/PKMζ*$^{(+/-)}$*Capn15*$^{(+/-)}$ mice and examined the eye phenotype of the offspring. As shown in Fig.8B, the *PKC/PKMζ*$^{(-/-)}$, *PKC/PKMζ*$^{(+/-)}$*Capn15*$^{(+/-)}$ and the *PKC/PKMζ*$^{(-/-)}$*Capn15*$^{(+/-)}$ mice generated from these crosses had no obvious eye deficits (Fig.8B). However, the *PKC/PKMζ*$^{(+/-)}$*Capn15*$^{(-/-)}$ mice generated from these crosses had cataracts (12.5%), microphthalmia (25%) and anophthalmia (12.5%) (n=10 for the *PKC/PKMζ*$^{(-/-)}$ group, n=22 for the *PKC/PKMζ*$^{(+/-)}$*Capn15*$^{(+/-)}$ group, n=12 for the *PKC/PKMζ*$^{(-/-)}$*Capn15*$^{(+/-)}$ group and n=8 for the *PKC/PKMζ*$^{(+/-)}$*Capn15*$^{(-/-)}$ group).

Discussion

While there are multiple classical and Tra calpains in most organisms, the SOL family of calpains consists of a single member present in all metazoan species (4). In *Aplysia*, blocking SOL calpain (Capn15) using a dominant negative construct blocked the induction of non-associative long term facilitation (43). SOL calpain was initially identified in *Drosophila* as a protease involved in optic lobe development (26). However, the functions of Capn15 in vertebrates are not well understood. In this paper, we have begun to characterize the function of Capn15 in mice by generating a KO model. By using lacZ reporter gene, we found that *Capn15* is mainly expressed in the developing central nervous system in E12 embryos at the mantle zone, which is at the opposing end of the ventricular zone. While the ventricular zone harbors neural progenitor cells undergoing proliferation, the mantle zone contains maturing neurons that are ready for differentiation (66). In E18 brains, *Capn15* is more concentrated in SVZ, where progenitor cells at this stage can give rise to both neurons and glial cells (67). Its expression in hippocampal neuroepithelial layer suggests a role in hippocampus development. *Capn15* was ubiquitously expressed in P3 brains while its expression was limited to the superficial cortical layer and was much more enriched in hippocampus in P100 brains. Although the identity of *Capn15* expressing cells is currently unknown due to inability of our Capn15 antibody to specifically recognize Capn15 in immunohistochemistry (no decrease in staining in KO animals), these results may indicate that Capn15 is involved in brain development by playing roles in multiple developmental processes.

The average weight of a whole *Capn15* KO mouse is 10% smaller compared to its WT littermate. Furthermore, MRI results showed that the *Capn15* KO brain is also 12% smaller in volume compared to the WT animals. This may indicate that the total 12% change in brain volume could be due to the proportional 10% weight loss, although there is no clear evidence that a decrease in overall weight necessarily leads to a decrease in brain volume. Nevertheless, certain brain areas such as subfields of the hippocampus and thalamus are still significantly smaller taking the 12A % global change into account. On the other hand, the amygdala is significantly larger in *Capn15* KO mice after scaling, indicating that this region is relatively spared.

Capn15 KO mice had striking eye deficits. *Capn15* is mapped to mouse chromosome 17A3.3 (28) which is a homologous region of human chromosome 16p13.3. In humans, patients with chromosomal translocation breaking at 16p13.3 present with CATM (hereditary cataracts with microphthalmia)(29), making *CAPN15* a candidate gene for this autosomal disorder (28) and our results support this idea. Unfortunately, it is not clear how *CAPN15* is associated with CATM on a cellular and molecular level, but Capn15 is expressed in different layers of retina as suggested by X-gal staining (Fig.2A). Multiple genes have been associated with microphthalmia/anophthalmia including *SOX2*, *OTX2*, *RAX*, *FOXE3* and *PAX6* (68). Many of these are transcription factors and CAPN15 may be involved in eye development through regulation of these genes, similar to the developmental role of other calpains in controlling transcription factors during development (11, 20, 25).

By screening fifty-six individuals (fifty-five independent families) from a UK cohort with eye anomalies, we identified a homozygous missense variant of *CAPN15* in

one patient. This variant is predicted to change Glycine 969, located in the SOL domain of *CAPN15,* into a Serine. While the amino acid substitution itself may be deleterious, it is also possible that the variant leads to mis-splicing. The nucleotide change affects the first nucleotide of the exon and converts it from the preferred CAG/G to CAG/A (69) potentially leading to exon skipping or an alternative exon entry. Sequencing of mRNA from the patient will be required to determine this.

Disruption of *PKC/PKMζ* in *Capn15* KO mice suppresses microphthalmia and anophthalmia. This suggests that Capn15 cleaves PKCζ during development and knocking-out *Capn15* causes an accumulation of PKCζ contributing to the severe eye deficits in *Capn15* KO mice. While most expression in the brain is of the alternative transcript *PKMζ*, the *PKCζ* transcript was found to be strongly expressed in the cuboidal epithelium and the pigment layer of the retina in developing E16.5 embryos suggesting it may play a role in eye development (70). Additional experiments are required to investigate this possibility. The findings reported in this study contribute to a better understanding of the genetic abnormalities underlying microphthalmia and may help in developing new therapies for this condition in the long term.

Acknowledgments

This work was supported by CIHR grant MOP 340328 to WSS. We would like to thank the families for their participation in our study. We are grateful to the West Midlands Regional Clinical Genetics Service, in particular Samuel Clokie and Shaun Green for their help with sample processing and clinical genetic testing of UK families with AMC conditions. This work was supported by grants from Baillie Gifford, Visually Impaired Children Taking Action (VICTA) (www.victa.org.uk), Microphthalmia, Anophthalmia and Coloboma Support (MACS) (www.macs.org.uk), and the HEIF (Health Innovation Fund, Oxford Brookes University).

Figure legends

Figure 1. Validation of the disruption of *Capn15*. (A) Breeding schematic to generate *Capn15* KO mice. Mice with lacZ and neo cassette are crossed to mice expressing FLP and the offspring are crossed to mice expressing germline Cre recombinase to remove the exons flanked by two loxP sites encoding the catalytic domain of Capn15. **(B)** Brains were homogenized and SDS-PAGE and western blotting were performed as described in Methods. Capn15 was probed using a rabbit anti-mouse Capn15 antibody. A band of ~130kDa corresponding to the expected molecular weight of Capn15 was detected in brain homogenates from wild type mice (*Capn15*$^{+/+}$) and this band was undetectable in *Capn15* KO mice (*Capn15*$^{-/-}$) .

Figure 2. *Capn15* is more enriched during early development. (A) X-gal staining of sections from E12, E18, P3 and P100 brains as well as sections from P3 eyes, hippocampus and cerebellum is shown. Scale bar is 200μm except for the magnified images of the hippocampus and the cerebellum where the scale bar is 100 μm. **(B)** Brains from rats at different developmental stages were homogenized and SDS-PAGE and western blotting were performed as described in Methods. This experiment was repeated three times. **(C)** Quantification of *Capn15* expression in rat brain. Capn15 expression was normalized to E12-E14 mice in each experiment; n=3 for E12-E14 group, n=4 for the

E16-E18 group, n=4 for the P0-P5 group, n=2 for the P30 group and n=3 for the P≥60 group. Error bars represent SEM.

Figure 3. Eye Phenotype of *Capn15* KO mice (A) Mendelian ratio of offspring from *Capn15* heterozygous parents. **(B)** Animals were weighed after weaning. Average weights of *Capn15 heterozygous* Capn15 KO mice were normalized to the average weight of WT mice. Error bars represent SEM. **(C)** Percentage of mice having eye deficits is compared in the WT, *Capn15* heterozygous and *Capn15* KO mice. Mice were grouped into 4 categories: Seems normal, obvious cataract, small eye and no eye and this scoring was performed on both left and right eye for each mouse. A Chi Square test revealed no significant difference in the eye phenotype distribution between the left eye and the right eye. Thus, the results from both eyes were combined for data analysis.

Figure 4. *Capn15* cKO mice have normal eyes. (A) Amygdala was dissected using a tissue puncher and homogenized and SDS-PAGE and western blotting were performed as described in Methods. **(B)** Quantification of *Capn15* expression in WT and *Capn15* cKO amygdala shows that Capn15 protein levels are significantly decreased in *Capn15* cKO adult mice amygdala. **(C)** Animals were weighed after weaning. Average weight of *Capn15* cKO was normalized to average weight of the WT mice. Error bars represent SEM. **(D)** Percentage of mice having eye deficits is compared between WT and *Capn15* cKO mice. Mice were grouped in 4 categories: Seems normal, obvious cataract, small eye and no eye and this scoring was performed on both left and right eye for each mouse. All of *Capn15* cKO mice eyes seemed normal.

Figure 5. Whole-brain visualization of significant decreases in brain structure volume for *Capn15* knockout (KO) mice compared to corresponding wild type (WT) mice. (A) The top two rows correspond to 20 axial sections through the mouse brain, the middle two rows correspond to 20 sagittal sections through the brain and the bottom two rows correspond to 20 coronal sections. Each section has a thickness of 100 micrometers. Blue/purple colours identify local voxel-level brain structure volume decrease calculated with a general linear model using a false discovery rate correction with a q-threshold of 0.05. **(B)** Box and whisker plots showing structure-specific brain volume differences between WT, KO and conditional knockout (cKO) mice. The left-most box and whisker plot labeled 'Scale' corresponds to measurements of whole-brain volume normalized to the atlas mouse brain.

Figure 6. Magnified coronal views through the mouse mid-brain displaying regional volume decrease (blue colours) and increase (orange) for *Capn15* KO mice compared to WT mice. Each slice through the mid-brain has a thickness of 100 micrometers. The specific position of each slice along the anterior-posterior axis of the mouse brain is shown, overlaid on a sagittal brain slice, in the top right hand corner of Figure 5. The colours represent t-statistical values calculated with a general linear model using a false discovery rate correction with a q-threshold of 0.05.

Figure 7. Hippocampal subfield-specific volume changes in *Capn15* KO and cKO mice relative to WT mice. (A) A hippocampal sub-field atlas (Badhwar et al.,

NeuroImage: Clinical, 2013) was applied to evaluate volumetric changes in the hippocampal subfields. The sub-field atlas includes region of interest labels demarcating the dentate gyrus (red), stratum granulosum (blue), CA1 (green), CA2 (purple) and CA3 (orange). **(B)** Box and whisker plots showing hippocampal subfield-specific volume differences between WT, KO and cKO mice.

Figure 8. Knocking-out *PKC/PKMζ* rescues the severe eye deficits in *Capn15* KO mice. Percentage of mice having eye deficits is compared in the *PKC/PKMζ*$^{(-/-)}$, *PKC/PKMζ*$^{(-/-)}$*Capn15*$^{(-/-)}$ and *Capn15*$^{(-/-)}$ mice from distinct litters **(A)** and in the *PKC/PKMζ* $^{(-/-)}$, *PKC/PKMζ* $^{(+/-)}$*Capn15*$^{(+/-)}$, *PKC/PKMζ*$^{(-/-)}$*Capn15*$^{(+/-)}$ and *PKC/PKMζ* $^{(+/-)}$*Capn15*$^{(-/-)}$ mice from the same litters **(B)**. Mice were grouped into 4 categories: Seems normal, obvious cataract, small eye and no eye and this scoring was performed on both left and right eye for each mouse. A Chi Square test revealed no significant difference in the eye phenoptype distribution between the left eye and the right eye. Thus, the results from both eyes were combined for data analysis.

References

1 Guroff, G. (1964) A Neutral, Calcium-Activated Proteinase from the Soluble Fraction of Rat Brain. *The Journal of biological chemistry*, **239**, 149-155.

2 Hastings, M.H., Qiu, A., Zha, C., Farah, C.A., Mahdid, Y., Ferguson, L. and Sossin, W.S. (2018) The zinc fingers of the small optic lobes calpain bind polyubiquitin. *Journal of neurochemistry*, **146**, 429-445.

3 Zhao, S., Liang, Z., Demko, V., Wilson, R., Johansen, W., Olsen, O.A. and Shalchian-Tabrizi, K. (2012) Massive expansion of the calpain gene family in unicellular eukaryotes. *BMC evolutionary biology*, **12**, 193.

4 Hastings, M.H., Gong, K., Freibauer, A., Courchesne, C., Fan, X. and Sossin, W.S. (2017) Novel calpain families and novel mechanisms for calpain regulation in Aplysia. *PloS one*, **12**, e0186646.

5 Shimizu, K., Phan, T., Mansuy, I.M. and Storm, D.R. (2007) Proteolytic degradation of SCOP in the hippocampus contributes to activation of MAP kinase and memory. *Cell*, **128**, 1219-1229.

6 Khoutorsky, A., Yanagiya, A., Gkogkas, C.G., Fabian, M.R., Prager-Khoutorsky, M., Cao, R., Gamache, K., Bouthiette, F., Parsyan, A., Sorge, R.E. *et al.* (2013) Control of synaptic plasticity and memory via suppression of poly(A)-binding protein. *Neuron*, **78**, 298-311.

7 Briz, V. and Baudry, M. (2017) Calpains: Master Regulators of Synaptic Plasticity. *The Neuroscientist : a review journal bringing neurobiology, neurology and psychiatry*, **23**, 221-231.

8 Smith, M.A. and Schnellmann, R.G. (2012) Calpains, mitochondria, and apoptosis. *Cardiovascular research*, **96**, 32-37.

9 Lebart, M.C. and Benyamin, Y. (2006) Calpain involvement in the remodeling of cytoskeletal anchorage complexes. *The FEBS journal*, **273**, 3415-3426.

10 Kerstein, P.C., Patel, K.M. and Gomez, T.M. (2017) Calpain-Mediated Proteolysis of Talin and FAK Regulates Adhesion Dynamics Necessary for Axon Guidance. *J Neurosci*, **37**, 1568-1580.

11 Abe, K. and Takeichi, M. (2007) NMDA-receptor activation induces calpain-mediated beta-catenin cleavages for triggering gene expression. *Neuron*, **53**, 387-397.

12 Potz, B.A., Abid, M.R. and Sellke, F.W. (2016) Role of Calpain in Pathogenesis of Human Disease Processes. *Journal of nature and science*, **2**.

13 Ono, Y. and Sorimachi, H. (2012) Calpains: an elaborate proteolytic system. *Biochimica et biophysica acta*, **1824**, 224-236.

14 Maki, M., Kitaura, Y., Satoh, H., Ohkouchi, S. and Shibata, H. (2002) Structures, functions and molecular evolution of the penta-EF-hand Ca2+-binding proteins. *Biochimica et biophysica acta*, **1600**, 51-60.

15 Liu, J., Liu, M.C. and Wang, K.K. (2008) Calpain in the CNS: from synaptic function to neurotoxicity. *Science signaling*, **1**, re1.

16 Bertipaglia, I. and Carafoli, E. (2007) Calpains and human disease. *Sub-cellular biochemistry*, **45**, 29-53.
17 Arthur, J.S. and Elce, J.S. (2000) Fluorescence measurements of Ca2+ binding to domain VI of calpain. *Methods Mol Biol*, **144**, 121-127.
18 Dutt, P., Croall, D.E., Arthur, J.S., Veyra, T.D., Williams, K., Elce, J.S. and Greer, P.A. (2006) m-Calpain is required for preimplantation embryonic development in mice. *BMC Dev Biol*, **6**, 3.
19 Hodgkin, J.A. and Brenner, S. (1977) Mutations causing transformation of sexual phenotype in the nematode Caenorhabditis elegans. *Genetics*, **86**, 275-287.
20 Sokol, S.B. and Kuwabara, P.E. (2000) Proteolysis in Caenorhabditis elegans sex determination: cleavage of TRA-2A by TRA-3. *Genes Dev*, **14**, 901-906.
21 Wang, S. and Kimble, J. (2001) The TRA-1 transcription factor binds TRA-2 to regulate sexual fates in Caenorhabditis elegans. *The EMBO journal*, **20**, 1363-1372.
22 Kammenga, J.E., Doroszuk, A., Riksen, J.A., Hazendonk, E., Spiridon, L., Petrescu, A.J., Tijsterman, M., Plasterk, R.H. and Bakker, J. (2007) A Caenorhabditis elegans wild type defies the temperature-size rule owing to a single nucleotide polymorphism in tra-3. *PLoS genetics*, **3**, e34.
23 Velez, G., Bassuk, A.G., Schaefer, K.A., Brooks, B., Gakhar, L., Mahajan, M., Kahn, P., Tsang, S.H., Ferguson, P.J. and Mahajan, V.B. (2018) A novel de novo CAPN5 mutation in a patient with inflammatory vitreoretinopathy, hearing loss, and developmental delay. *Cold Spring Harb Mol Case Stud*, **4**.
24 Denison, S.H., Orejas, M. and Arst, H.N., Jr. (1995) Signaling of ambient pH in Aspergillus involves a cysteine protease. *The Journal of biological chemistry*, **270**, 28519-28522.
25 Penas, M.M., Hervas-Aguilar, A., Munera-Huertas, T., Reoyo, E., Penalva, M.A., Arst, H.N., Jr. and Tilburn, J. (2007) Further characterization of the signaling proteolysis step in the Aspergillus nidulans pH signal transduction pathway. *Eukaryot Cell*, **6**, 960-970.
26 Delaney, S.J., Hayward, D.C., Barleben, F., Fischbach, K.F. and Miklos, G.L. (1991) Molecular cloning and analysis of small optic lobes, a structural brain gene of Drosophila melanogaster. *Proceedings of the National Academy of Sciences of the United States of America*, **88**, 7214-7218.
27 Fischbach, K.F. and Heisenberg, M. (1981) Structural brain mutant of Drosophila melanogaster with reduced cell number in the medulla cortex and with normal optomotor yaw response. *Proceedings of the National Academy of Sciences of the United States of America*, **78**, 1105-1109.
28 Kamei, M., Webb, G.C., Young, I.G. and Campbell, H.D. (1998) SOLH, a human homologue of the Drosophila melanogaster small optic lobes gene is a member of the calpain and zinc-finger gene families and maps to human chromosome 16p13.3 near CATM (cataract with microphthalmia). *Genomics*, **51**, 197-206.
29 Yokoyama, Y., Narahara, K., Tsuji, K., Ninomiya, S. and Seino, Y. (1992) Autosomal dominant congenital cataract and microphthalmia associated with a familial t(2;16) translocation. *Hum Genet*, **90**, 177-178.
30 Moldoveanu, T., Hosfield, C.M., Lim, D., Elce, J.S., Jia, Z. and Davies, P.L. (2002) A Ca(2+) switch aligns the active site of calpain. *Cell*, **108**, 649-660.
31 Pastalkova, E., Serrano, P., Pinkhasova, D., Wallace, E., Fenton, A.A. and Sacktor, T.C. (2006) Storage of spatial information by the maintenance mechanism of LTP. *Science*, **313**, 1141-1144.
32 Cai, D., Pearce, K., Chen, S. and Glanzman, D.L. (2011) Protein kinase M maintains long-term sensitization and long-term facilitation in aplysia. *J Neurosci*, **31**, 6421-6431.
33 Balaban, P.M., Roshchin, M., Timoshenko, A., Zuzina, A.B., Lemak, M., Ierusalimsky, V.N., Aseyev, N.A. and Malyshev, A.Y. (2015) Homolog of protein kinase Mzeta maintains context

aversive memory and underlying long-term facilitation in terrestrial snail Helix. *Front Cell Neurosci*, **9**, 222.
34 Drier, E.A., Tello, M.K., Cowan, M., Wu, P., Blace, N., Sacktor, T.C. and Yin, J.C. (2002) Memory enhancement and formation by atypical PKM activity in Drosophila melanogaster. *Nature neuroscience*, **5**, 316-324.
35 Nikitin, V.P., Solntseva, S.V., Kozyrev, S.A., Nikitin, P.V. and Shevelkin, A.V. (2016) Different components of conditioned food aversion memory. *Brain research*, **1642**, 104-113.
36 Shema, R., Haramati, S., Ron, S., Hazvi, S., Chen, A., Sacktor, T.C. and Dudai, Y. (2011) Enhancement of consolidated long-term memory by overexpression of protein kinase Mzeta in the neocortex. *Science*, **331**, 1207-1210.
37 Serrano, P., Friedman, E.L., Kenney, J., Taubenfeld, S.M., Zimmerman, J.M., Hanna, J., Alberini, C., Kelley, A.E., Maren, S., Rudy, J.W. *et al.* (2008) PKMzeta maintains spatial, instrumental, and classically conditioned long-term memories. *PLoS biology*, **6**, 2698-2706.
38 Menzel, R. (2001) Searching for the memory trace in a mini-brain, the honeybee. *Learning & memory*, **8**, 53-62.
39 Hernandez, A.I., Blace, N., Crary, J.F., Serrano, P.A., Leitges, M., Libien, J.M., Weinstein, G., Tcherapanov, A. and Sacktor, T.C. (2003) Protein kinase M zeta synthesis from a brain mRNA encoding an independent protein kinase C zeta catalytic domain. Implications for the molecular mechanism of memory. *The Journal of biological chemistry*, **278**, 40305-40316.
40 Bougie, J.K., Lim, T., Farah, C.A., Manjunath, V., Nagakura, I., Ferraro, G.B. and Sossin, W.S. (2009) The atypical protein kinase C in Aplysia can form a protein kinase M by cleavage. *Journal of neurochemistry*, **109**, 1129-1143.
41 Bougie, J.K., Cai, D., Hastings, M., Farah, C.A., Chen, S., Fan, X., McCamphill, P.K., Glanzman, D.L. and Sossin, W.S. (2012) Serotonin-induced cleavage of the atypical protein kinase C Apl III in Aplysia. *J Neurosci*, **32**, 14630-14640.
42 Farah, C.A., Hastings, M.H., Dunn, T.W., Gong, K., Baker-Andresen, D. and Sossin, W.S. (2017) A PKM generated by calpain cleavage of a classical PKC is required for activity-dependent intermediate-term facilitation in the presynaptic sensory neuron of Aplysia. *Learning & memory*, **24**, 1-13.
43 Hu, J., Adler, K., Farah, C.A., Hastings, M.H., Sossin, W.S. and Schacher, S. (2017) Cell-Specific PKM Isoforms Contribute to the Maintenance of Different Forms of Persistent Long-Term Synaptic Plasticity. *J Neurosci*, **37**, 2746-2763.
44 Sossin, W.S. (2003) Phosphopeptide-specific antibodies to protein kinase C. *Methods Mol Biol*, **233**, 233-244.
45 Nakhost, A., Forscher, P. and Sossin, W.S. (1998) Binding of protein kinase C isoforms to actin in Aplysia. *Journal of neurochemistry*, **71**, 1221-1231.
46 Collins, D.L., Neelin, P., Peters, T.M. and Evans, A.C. (1994) Automatic 3D intersubject registration of MR volumetric data in standardized Talairach space. *J Comput Assist Tomogr*, **18**, 192-205.
47 Kovacevic, N., Henderson, J.T., Chan, E., Lifshitz, N., Bishop, J., Evans, A.C., Henkelman, R.M. and Chen, X.J. (2005) A three-dimensional MRI atlas of the mouse brain with estimates of the average and variability. *Cereb Cortex*, **15**, 639-645.
48 Fonov, V., Evans, A.C., Botteron, K., Almli, C.R., McKinstry, R.C., Collins, D.L. and Brain Development Cooperative, G. (2011) Unbiased average age-appropriate atlases for pediatric studies. *Neuroimage*, **54**, 313-327.
49 Avants, B.B., Epstein, C.L., Grossman, M. and Gee, J.C. (2008) Symmetric diffeomorphic image registration with cross-correlation: evaluating automated labeling of elderly and neurodegenerative brain. *Med Image Anal*, **12**, 26-41.

50 Badhwar, A., Lerch, J.P., Hamel, E. and Sled, J.G. (2013) Impaired structural correlates of memory in Alzheimer's disease mice. *Neuroimage Clin*, **3**, 290-300.
51 Pinheiro, J. and Bates D. (2000) *Mixed-Effects Models in S and S-PLUS*. Springer.
52 Genovese, C.R., Lazar, N.A. and Nichols, T. (2002) Thresholding of statistical maps in functional neuroimaging using the false discovery rate. *Neuroimage*, **15**, 870-878.
53 Holt, R.J., Young, R.M., Crespo, B., Ceroni, F., Curry, C.J., Bellacchio, E., Bax, D.A., Ciolfi, A., Simon, M., Fagerberg, C.R. *et al.* (2019) De Novo Missense Variants in FBXW11 Cause Diverse Developmental Phenotypes Including Brain, Eye, and Digit Anomalies. *American journal of human genetics*, in press.
54 Ragge, N., Isidor, B., Bitoun, P., Odent, S., Giurgea, I., Cogne, B., Deb, W., Vincent, M., Le Gall, J., Morton, J. *et al.* (2019) Expanding the phenotype of the X-linked BCOR microphthalmia syndromes. *Hum Genet*, **138**, 1051-1069.
55 Brown, S.D. and Moore, M.W. (2012) The International Mouse Phenotyping Consortium: past and future perspectives on mouse phenotyping. *Mamm Genome*, **23**, 632-640.
56 Skarnes, W.C., Rosen, B., West, A.P., Koutsourakis, M., Bushell, W., Iyer, V., Mujica, A.O., Thomas, M., Harrow, J., Cox, T. *et al.* (2011) A conditional knockout resource for the genome-wide study of mouse gene function. *Nature*, **474**, 337-342.
57 Tsien, J.Z., Chen, D.F., Gerber, D., Tom, C., Mercer, E.H., Anderson, D.J., Mayford, M., Kandel, E.R. and Tonegawa, S. (1996) Subregion- and cell type-restricted gene knockout in mouse brain. *Cell*, **87**, 1317-1326.
58 Li, Y., Stam, F.J., Aimone, J.B., Goulding, M., Callaway, E.M. and Gage, F.H. (2013) Molecular layer perforant path-associated cells contribute to feed-forward inhibition in the adult dentate gyrus. *Proceedings of the National Academy of Sciences of the United States of America*, **110**, 9106-9111.
59 Armstrong, C., Szabadics, J., Tamas, G. and Soltesz, I. (2011) Neurogliaform cells in the molecular layer of the dentate gyrus as feed-forward gamma-aminobutyric acidergic modulators of entorhinal-hippocampal interplay. *J Comp Neurol*, **519**, 1476-1491.
60 Sonner, J.M., Cascio, M., Xing, Y., Fanselow, M.S., Kralic, J.E., Morrow, A.L., Korpi, E.R., Hardy, S., Sloat, B., Eger, E.I., 2nd *et al.* (2005) Alpha 1 subunit-containing GABA type A receptors in forebrain contribute to the effect of inhaled anesthetics on conditioned fear. *Molecular pharmacology*, **68**, 61-68.
61 Hu, J., Ferguson, L., Adler, K., Farah, C.A., Hastings, M.H., Sossin, W.S. and Schacher, S. (2017) Selective Erasure of Distinct Forms of Long-Term Synaptic Plasticity Underlying Different Forms of Memory in the Same Postsynaptic Neuron. *Current biology : CB*, **27**, 1888-1899 e1884.
62 Adzhubei, I.A., Schmidt, S., Peshkin, L., Ramensky, V.E., Gerasimova, A., Bork, P., Kondrashov, A.S. and Sunyaev, S.R. (2010) A method and server for predicting damaging missense mutations. *Nat Methods*, **7**, 248-249.
63 Lek, M., Karczewski, K.J., Minikel, E.V., Samocha, K.E., Banks, E., Fennell, T., O'Donnell-Luria, A.H., Ware, J.S., Hill, A.J., Cummings, B.B. *et al.* (2016) Analysis of protein-coding genetic variation in 60,706 humans. *Nature*, **536**, 285-291.
64 Ng, P.C. and Henikoff, S. (2003) SIFT: Predicting amino acid changes that affect protein function. *Nucleic Acids Res*, **31**, 3812-3814.
65 Sacktor, T.C. (2012) Memory maintenance by PKMzeta--an evolutionary perspective. *Molecular brain*, **5**, 31.
66 Thompson, C.L., Ng, L., Menon, V., Martinez, S., Lee, C.K., Glattfelder, K., Sunkin, S.M., Henry, A., Lau, C., Dang, C. *et al.* (2014) A high-resolution spatiotemporal atlas of gene expression of the developing mouse brain. *Neuron*, **83**, 309-323.

67 Levers, T.E., Edgar, J.M. and Price, D.J. (2001) The fates of cells generated at the end of neurogenesis in developing mouse cortex. *Journal of neurobiology*, **48**, 265-277.
68 Plaisancie, J., Ceroni, F., Holt, R., Zazo Seco, C., Calvas, P., Chassaing, N. and Ragge, N.K. (2019) Genetics of anophthalmia and microphthalmia. Part 1: Non-syndromic anophthalmia/microphthalmia. *Hum Genet*, in press.
69 Mount, S.M. (1982) A catalogue of splice junction sequences. *Nucleic Acids Res*, **10**, 459-472.
70 Kovac, J., Oster, H. and Leitges, M. (2007) Expression of the atypical protein kinase C (aPKC) isoforms iota/lambda and zeta during mouse embryogenesis. *Gene Expr Patterns*, **7**, 187-196.

Figure 1

A

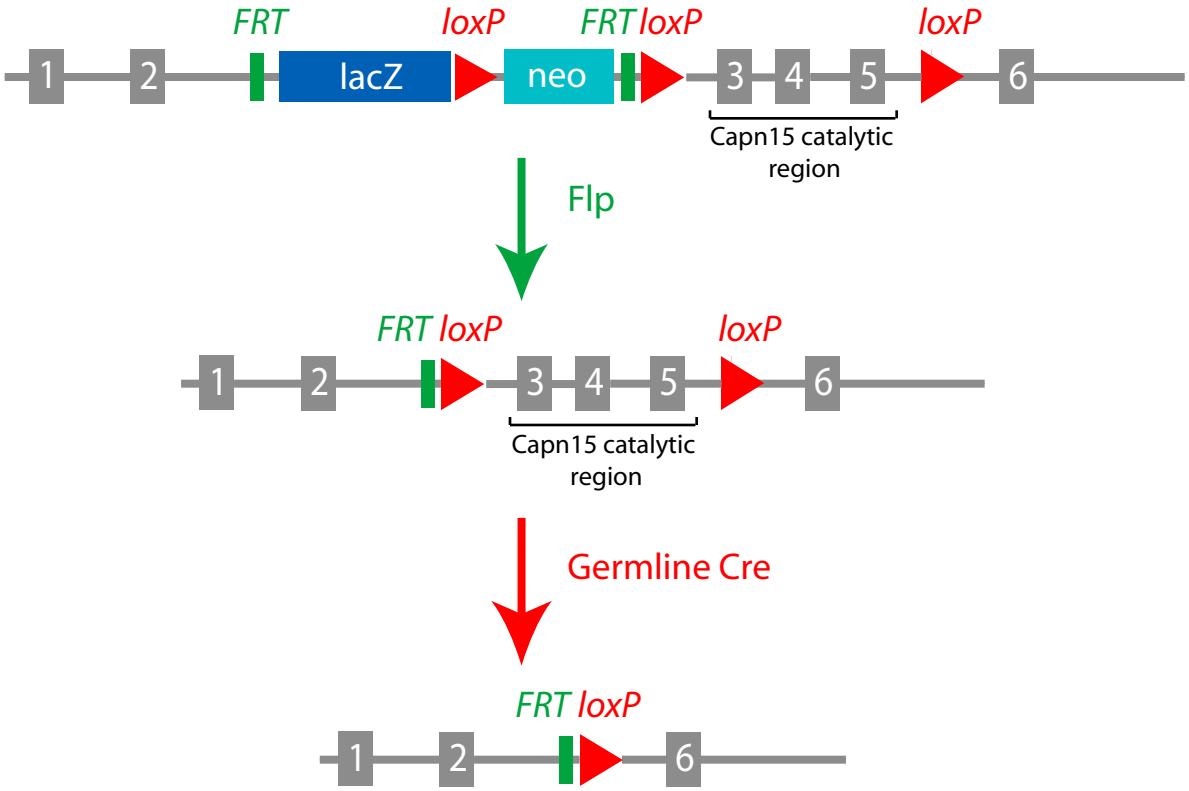
FRT
loxP
FRT loxP
loxP
1
2
lacZ
neo
3
4
5
6
Capn15 catalytic region
Flp
FRT loxP
loxP
1
2
3
4
5
6
Capn15 catalytic region
Germline Cre
FRT loxP
1
2
6

B

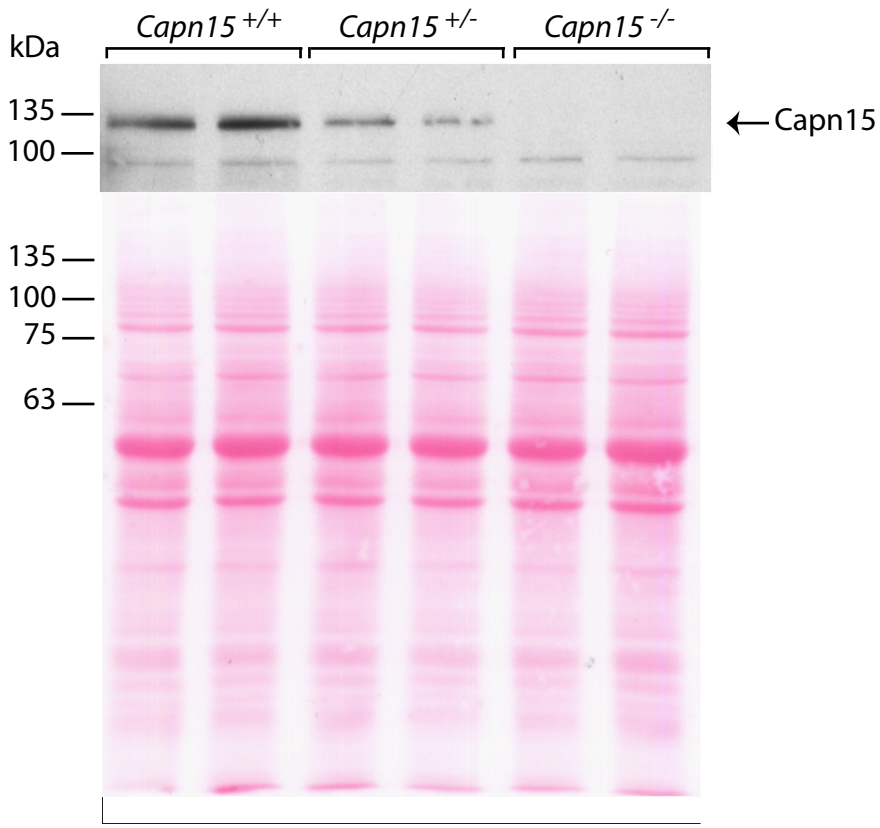
kDa
Capn15 +/+
Capn15 +/-
Capn15 -/-
135
100
Capn15
135
100
75
63

Figure 2

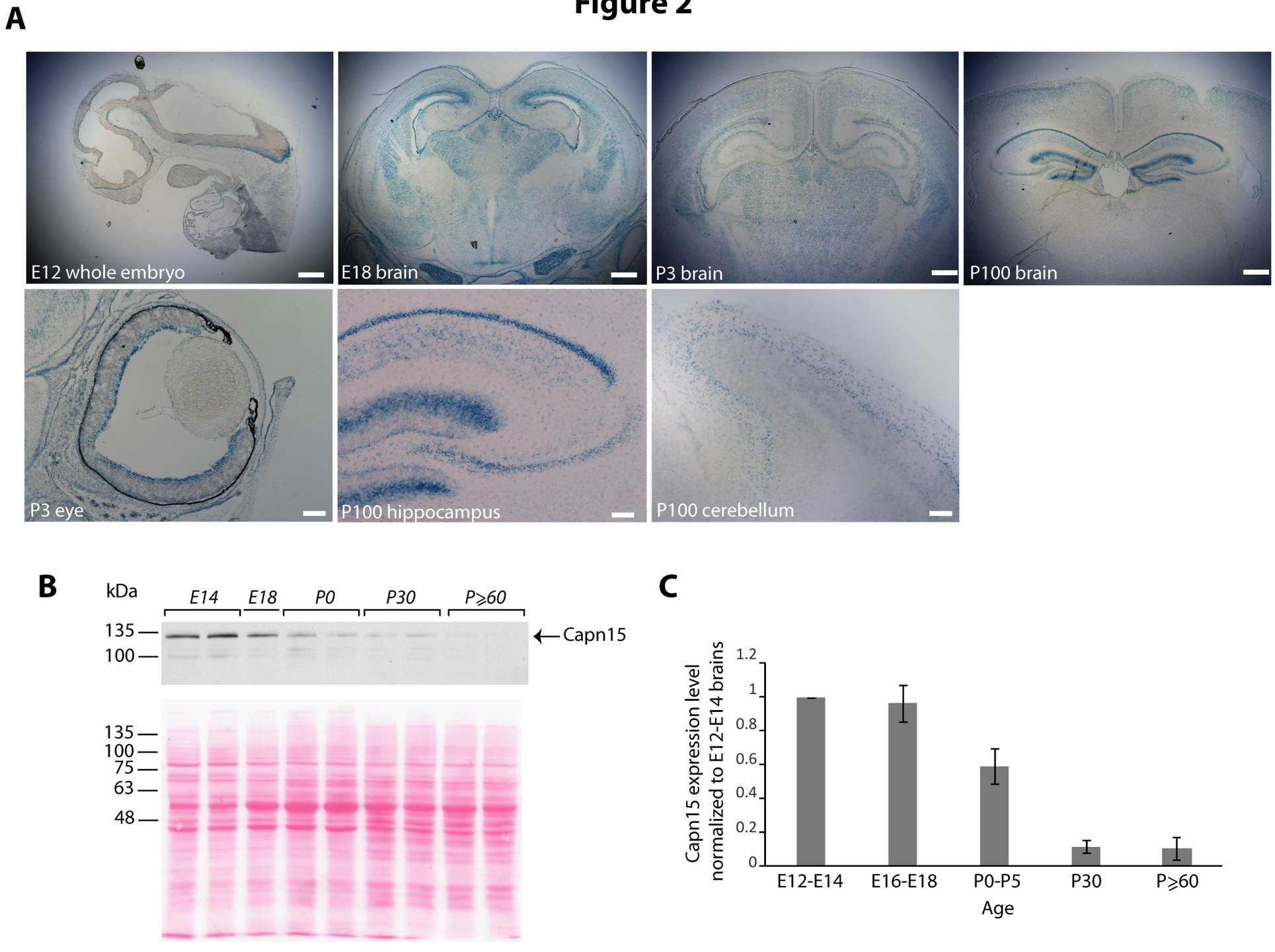
A
E12 whole embryo
E18 brain
P3 brain
P100 brain
P3 eye
P100 hippocampus
P100 cerebellum
B
kDa
E14
E18
P0
P30
P≥60
135
100
Capn15
135
100
75
63
48
C
Capn15 expression level normalized to E12-E14 brains
1.2
1
0.8
0.6
0.4
0.2
0
E12-E14
E16-E18
P0-P5
P30
P≥60
Age

Figure 3

A

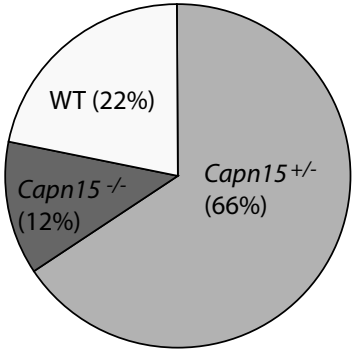
WT (22%)
Capn15 -/- (12%)
Capn15 +/- (66%)

B

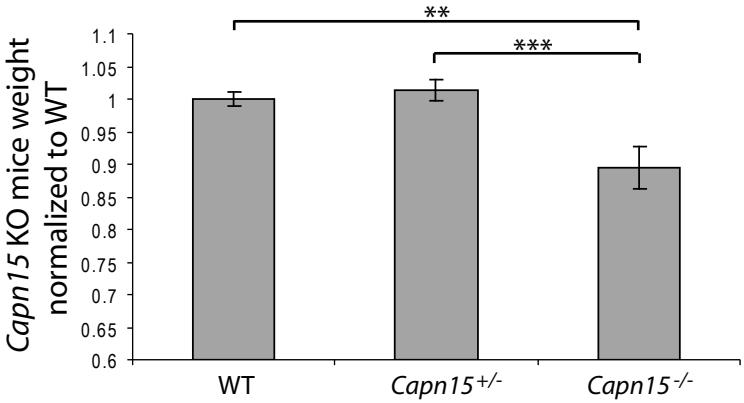
**
***
Capn15 KO mice weight normalized to WT
1.1
1.05
1
0.95
0.9
0.85
0.8
0.75
0.7
0.65
0.6
WT
Capn15+/-
Capn15-/-

C

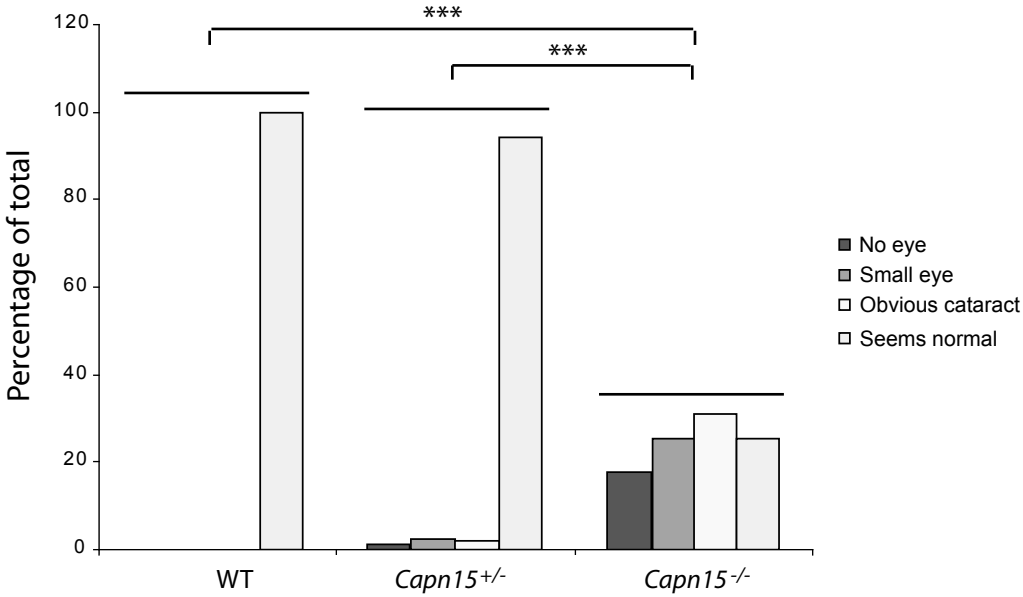
***
***
Percentage of total
120
100
80
60
40
20
0
WT
Capn15+/-
Capn15-/-
No eye
Small eye
Obvious cataract
Seems normal

Figure 4

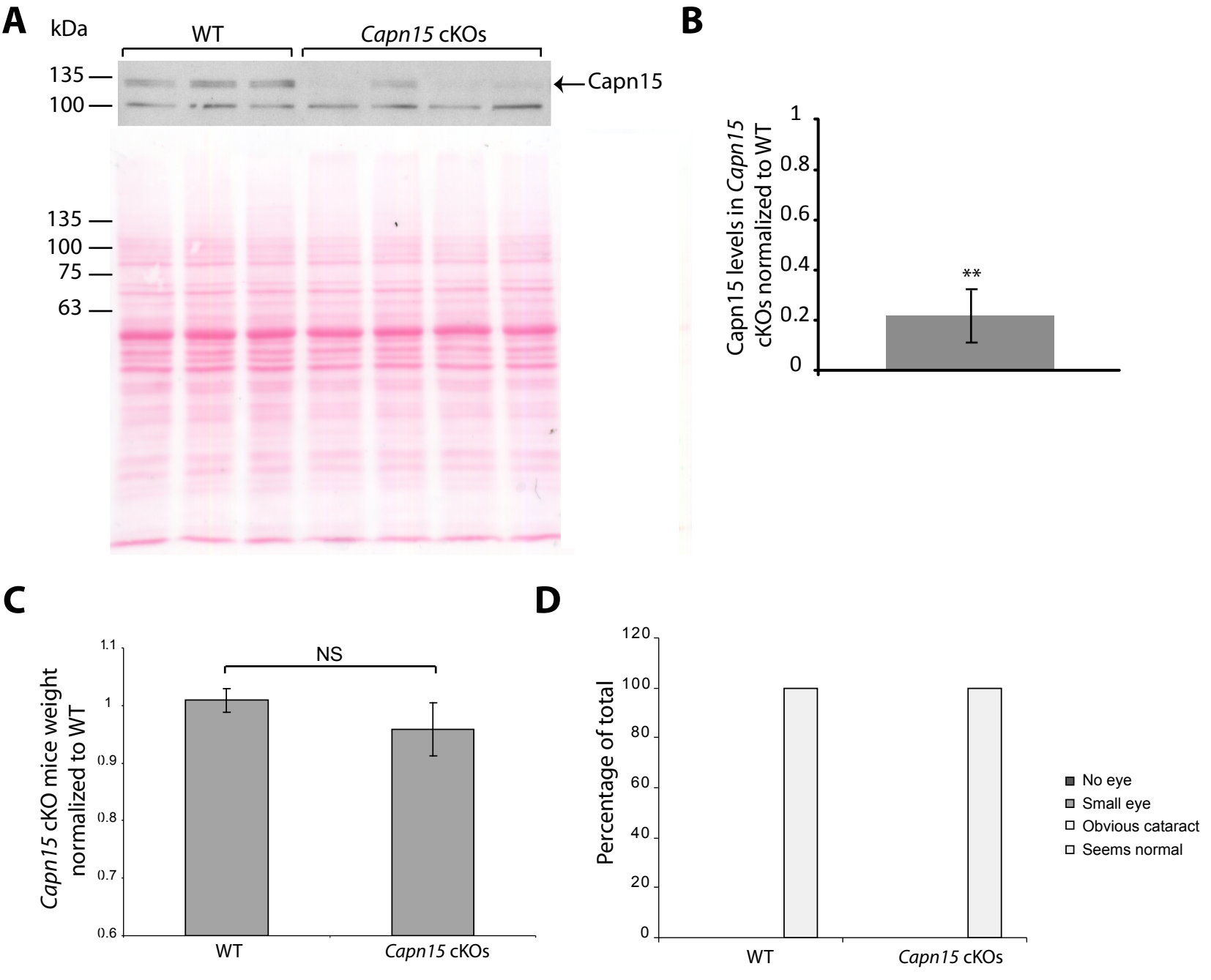
A
kDa
WT
Capn15 cKOs
135
100
Capn15
135
100
75
63
B
Capn15 levels in Capn15 cKOs normalized to WT
1
0.8
0.6
0.4
0.2
0
**
C
Capn15 cKO mice weight normalized to WT
1.1
1
0.9
0.8
0.7
0.6
NS
WT
Capn15 cKOs
D
Percentage of total
120
100
80
60
40
20
0
WT
Capn15 cKOs
No eye
Small eye
Obvious cataract
Seems normal

Figure 5

A

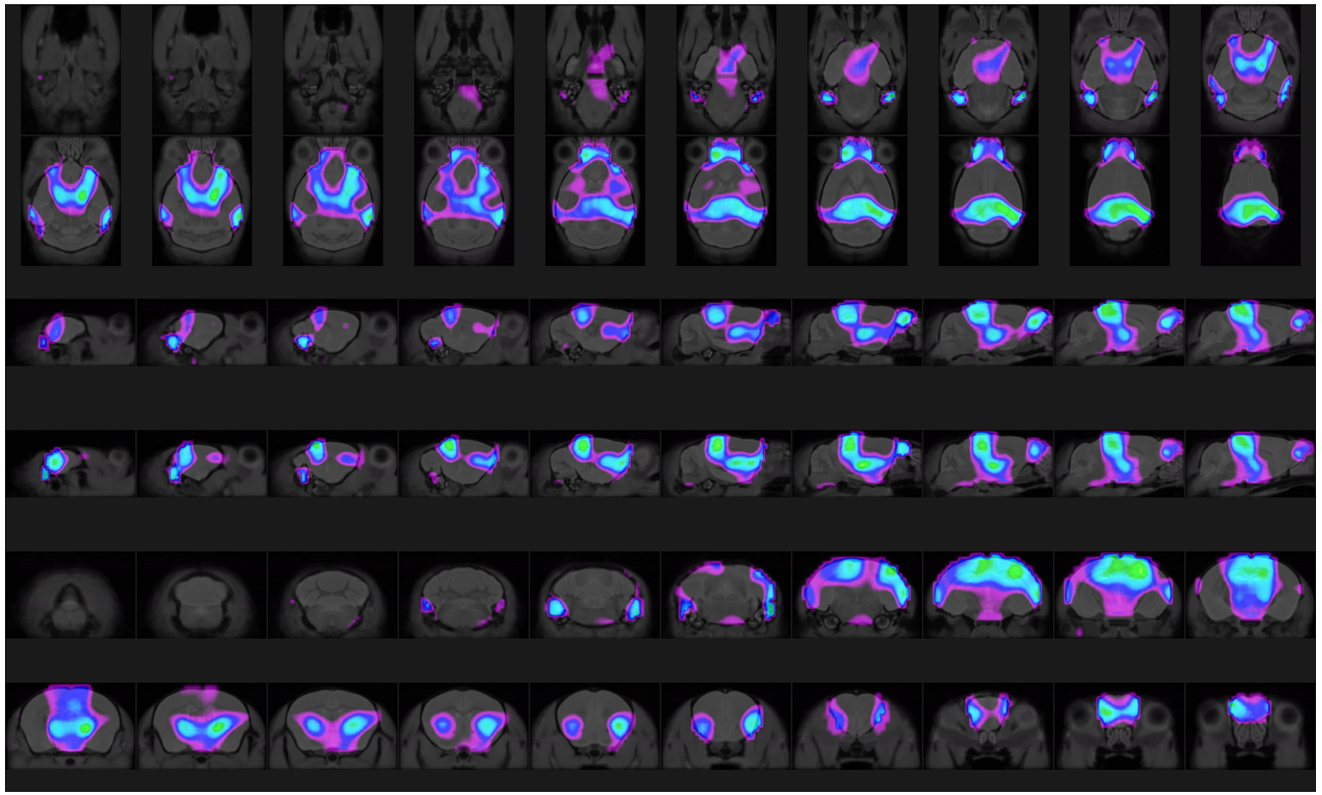

B

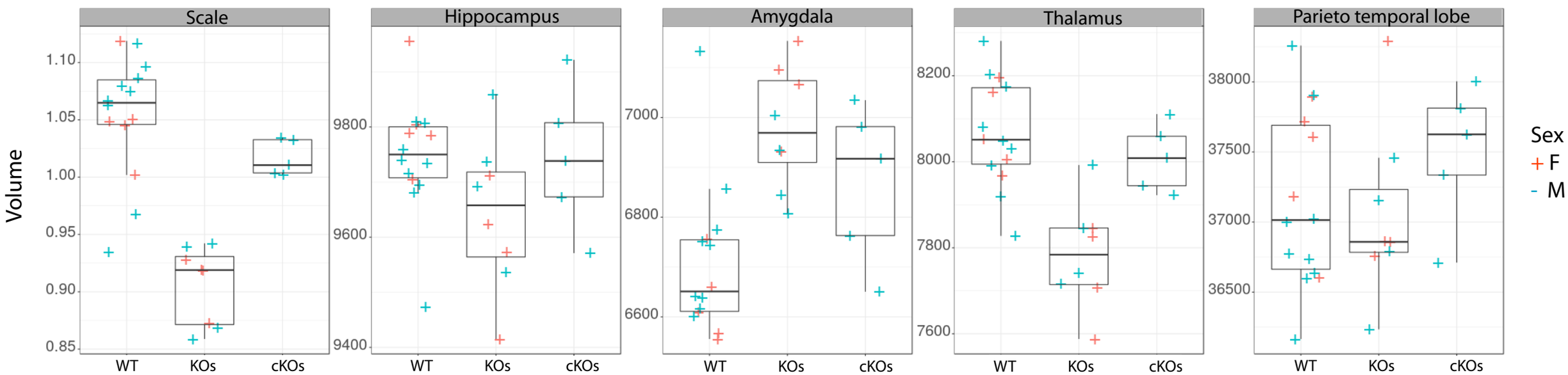
Scale
Hippocampus
Amygdala
Thalamus
Parieto temporal lobe
Volume
1.10
1.05
1.00
0.95
0.90
0.85
9800
9600
9400
7000
6800
6600
8200
8000
7800
7600
38000
37500
37000
36500
WT
KOs
cKOs
Sex
F
M

Figure 6

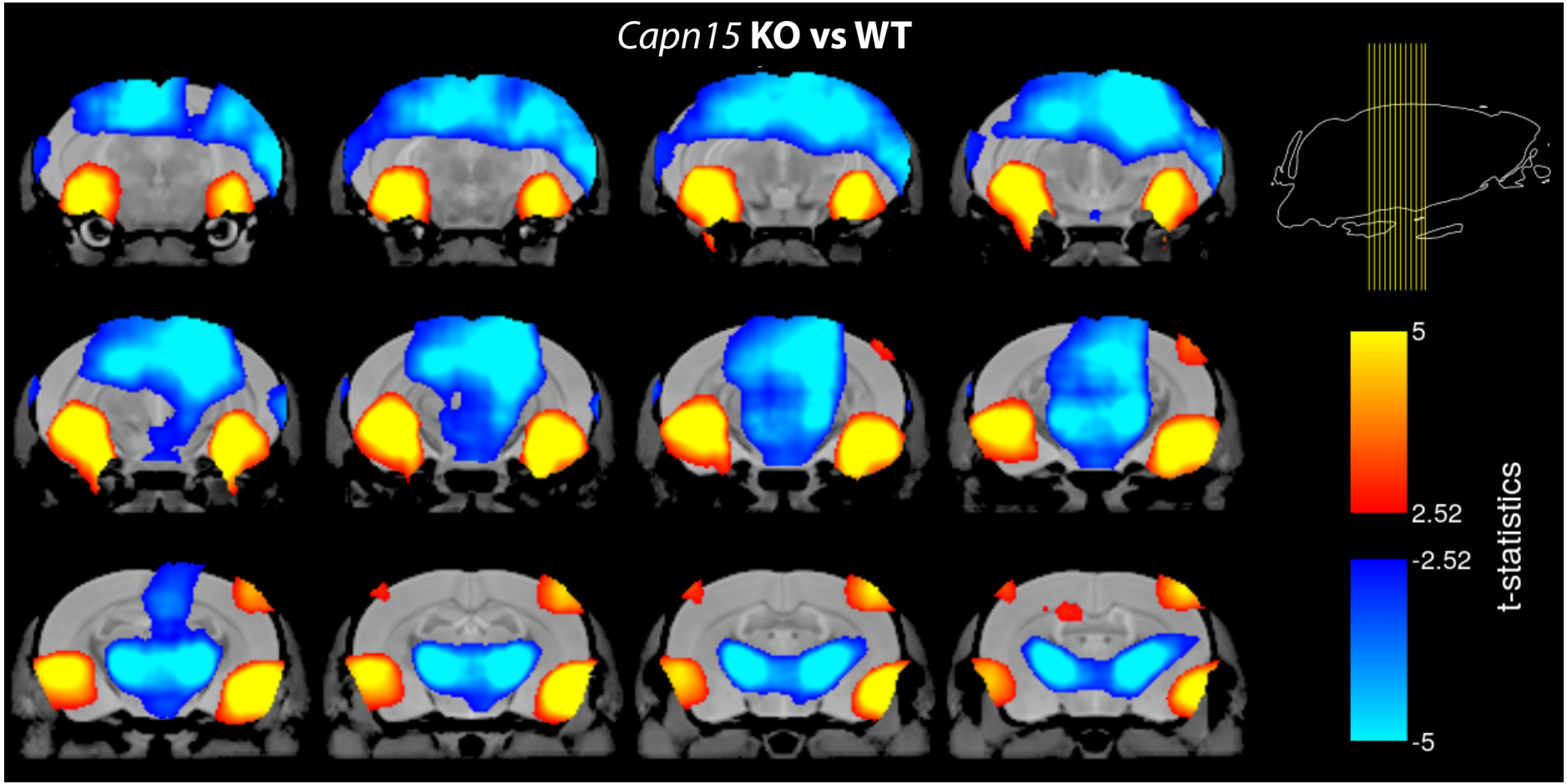

Figure 7

A

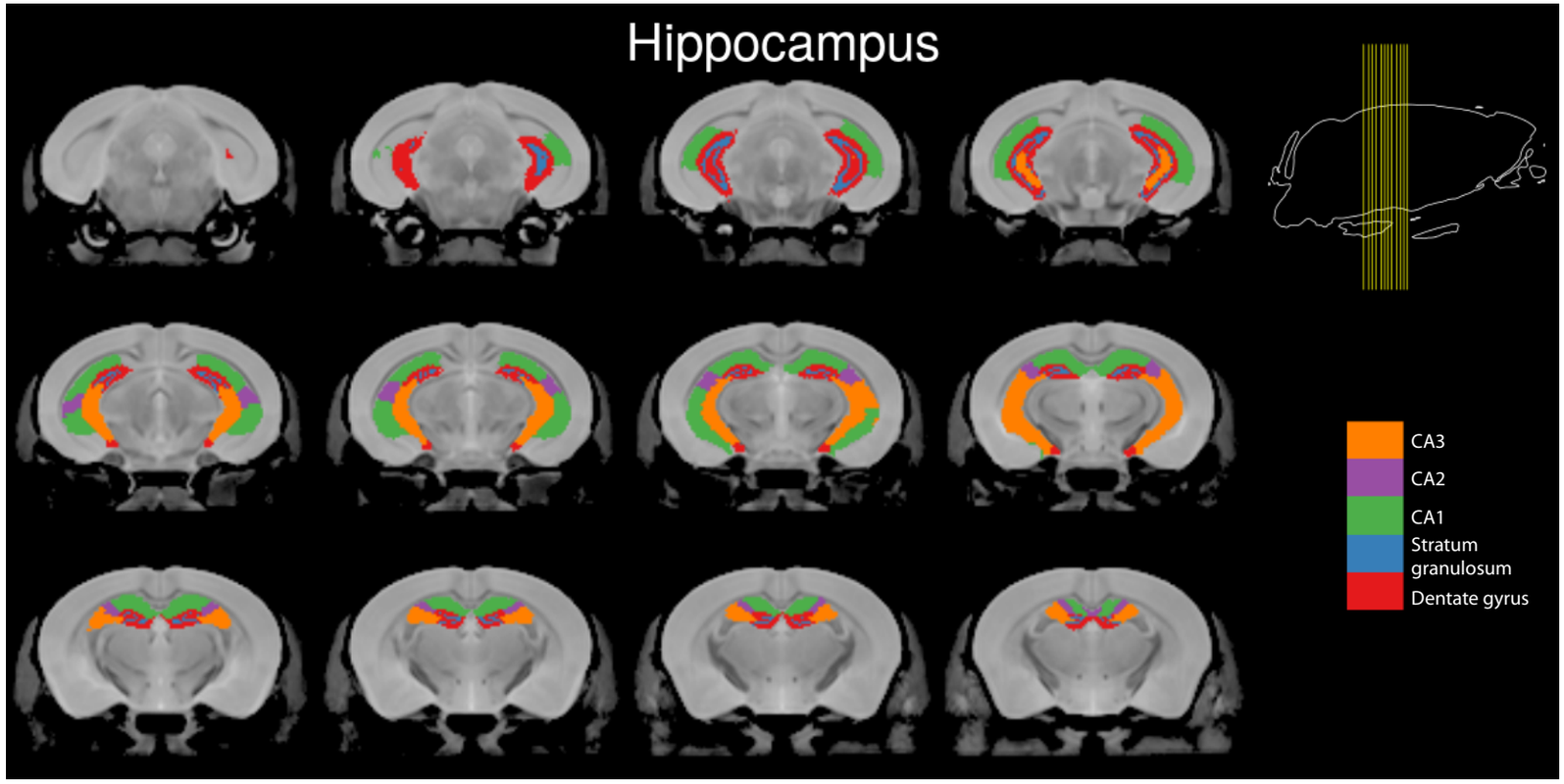
Hippocampus
CA3
CA2
CA1
Stratum granulosum
Dentate gyrus

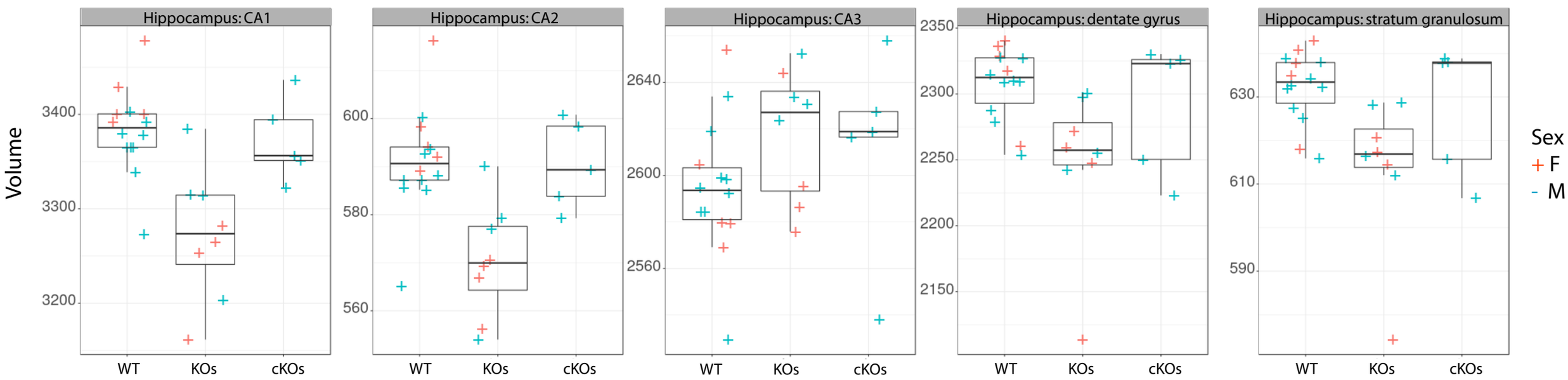
Hippocampus: CA1
Hippocampus: CA2
Hippocampus: CA3
Hippocampus: dentate gyrus
Hippocampus: stratum granulosum
Volume
3400
3300
3200
600
580
560
2640
2600
2560
2350
2300
2250
2200
2150
630
610
590
WT
KOs
cKOs
Sex
+ F
- M

Figure 8

A

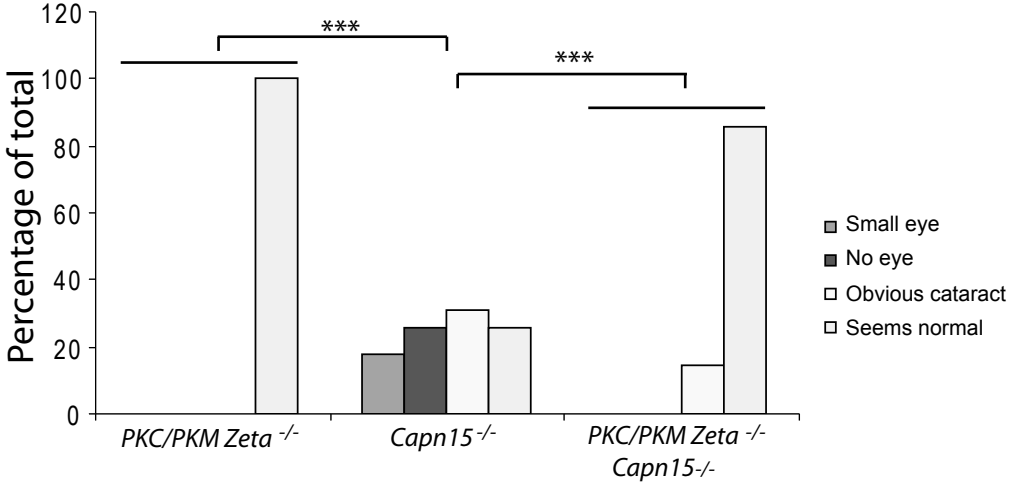
120
100
80
60
40
20
0
Percentage of total
***
***
Small eye
No eye
Obvious cataract
Seems normal
PKC/PKM Zeta -/-
Capn15 -/-
PKC/PKM Zeta -/-
Capn15-/-

B

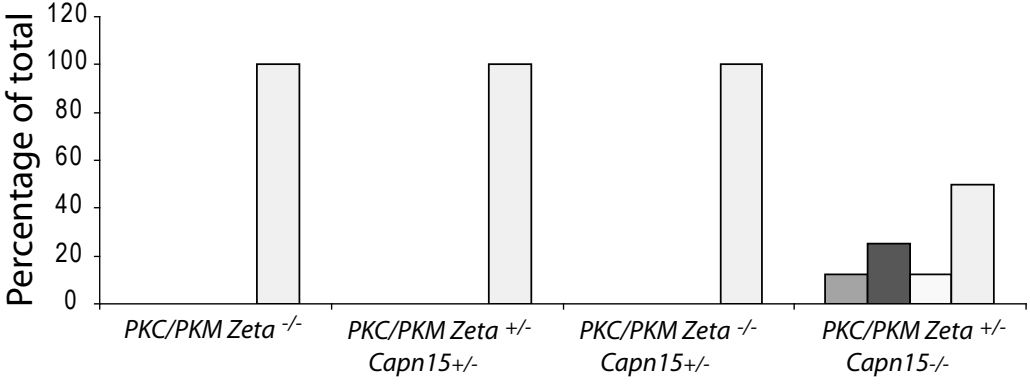
120
100
80
60
40
20
0
Percentage of total
PKC/PKM Zeta -/-
PKC/PKM Zeta +/-
Capn15+/-
PKC/PKM Zeta -/-
Capn15+/-
PKC/PKM Zeta +/-
Capn15-/-